

Exploration of Long-Range Surface Plasmon Resonance on multilayer single mode optical fiber with function of MgF₂

*R. Zakaria¹, N.A.M. Zainuddin¹, M.A.S. Ahmad Fahri¹, Amrita Kamkar², Fahad Ahmed Al Zahrani³, Shobhit K. Patel⁴ and Kawsar Ahmed^{2,5}

¹Photonics Research Centre, Faculty Science, University of Malaya, Lembah Pantai, 50603 Kuala Lumpur, Malaysia

²Department of Information and Communication Technology, Mawlana Bhashani Science and Technology University, Santosh, Tangail-1902, Bangladesh

³Computer Engineering Department, Umm Al-Qura University, Mecca 24381, Saudi Arabia

⁴Department of Physics and Department of ECE, Marwadi University, Rajkot 360003, India

⁵Group of Bio-photomatrix, Mawlana Bhashani Science and Technology University, Santosh, Tangail-1902, Bangladesh

Corresponding address: rozalina@um.edu.my

Abstract: Multilayer models for single mode optical fiber based on Long Range Surface Plasmon Resonance (LRSPR) coated with silver (Ag) and gold (Au) with dielectric function of MgF₂ are introduced. Properties for the models are theoretically and experimentally reported in this work. Firstly, the performances of different models are investigated using COMSOL simulation. Different combinations of magnesium fluoride (MgF₂) and Ag/Au material embedded layers are applied to observed functionality of dielectric layers underneath the analyte. In theoretical analysis, MgF₂-Ag and MgF₂-Ag-MgF₂ layers conveys the best performance in sensing. The combination of plasmonic material Ag with MgF₂ rather than Au shows higher sensitivity response. The experimental has been carried out with these configurations where exhibit the sensitivities of 1762.5 nm/RIU and 1250 nm/RIU at 1.37-1.38 and 1.33-1.34 RI range respectively for silver-based models. The outcomes indicate the proposed LRSPR based models with specific dielectric where here MgF₂ found to be a strong match in sensing applications.

Keywords: Analyte Sensitivity, D-Shaped LRSPR; MgF₂; RI sensor.

1. Introduction

Surface plasmon resonance has already proved its potentiality in research field where integrated of SPR performs a vital role in nonlinear and modern optics for thin metal film processing. It is also a fundamental of many efficient tools for standard assessment of molecular absorption such as Polymers, DNA or proteins. SPR is an interface of electrons between real and imaginary permittivity where SPs (Surface Plasmons) are the interface of charge density between metal and dielectric [1]. Theoretically, if a dielectric material in SPR configuration is coated with thin film of metal then it propagates Surface plasmon waves (SPw) [2]. Surface Plasmons are electromagnetic waves generated by corporate oscillation of conducted electrons. These are mostly supported by the metals like Ag and Au where other metals like (Copper, Titanium, Chromium, Alkali, Subalkali etc.) also have some impacts to create SPR [3]. Among the different versions of SPR, Long Range Surface Plasmon is another technique to enhance the performance of SPR. During the last decade, the Long-Range Surface Plasmon resonance (LR-SPR) has got tremendous cognizance from the researchers, where most researchers found it feasible to improve the sensor's execution [4].

Therefore, the technique of LRSPR has been used in diverse applications, including nonlinear interaction, molecular fluorescent, Raman spectroscopy, transmission through metal films, emission extraction, amplification, surface characterization, optical interconnections with integrated structures, thermo-electro, magneto-optics and chemical sensing [5]. Competitive features for these examples extend propagating length and stronger electric field on surface, confined wavelength, which induce larger infiltrated evanescent depth in the sensing medium [6]. Apart from the Surface Plasmons (SPs) the Long-Range Surface Plasmons (LRSPs) are taken for finding a long propagating distance with strongly associated configuration for local field [7]. When the light occurrence along with individual electrons satisfies the condition called phase matching, energy of this light occurrence is opposed to the SPP mode [8]. When this stated model use the similar RI, Surface Plasmon Polaritons (SPP) of metals coupled into two different coupling modes. One is Long Range Surface Plasmon Polariton (LRSPR) and another is Short Range Surface Plasmon Polariton (SRSPR). The reflection of spectrum compared to the normal one gives lower loss and extended propagating length, which presents a confined SPR dip. Augmentation is then called Long Range Surface Plasmon Resonance (LRSPR).

Long-range and short-range are considered as two resonance dips of LRSPR sensor's resonance spectra. As the loss of LRSPR is less than the SRSPR, the resonance dip for Long range is

narrower as well as deeper than the short-range resonance dip. Hence, to characterize the LRSPR sensor performance long-range resonance dips are used [9]. Improving RI sensor is also a purpose of LRSPR study. In Long-Range Surface Plasmon Resonance, the refractive index changes near the surface of the sensor. This mode of SPR offers absolute opportunity to cut out the features for metallic surface [10]. That means LRSPR would provide an opportunity to derive metal composition on surface. Keeping all parameters constant, the angle of SPR is absolutely sensitive to move by the change of RI with a thin film to the metal surface. In a metal film, coupling between SPs opposite to the films can occur by increasing symmetric and antisymmetric SPs [11] mixed modes for electromagnetic. The initiated shift of SPR angle indicates the SPR signal millidegree or RIU (RI unit) equal to the concentration of binding event on the sensor chip surface [12]. Limited sensitivity detection is considered to be a drawback of SPR. To overcome this problem, using dielectric or nanoparticle plasmonic labeled analyte are used to precise the SPR signal.

As a dielectric, MgF_2 has grabbed wide attention with its less refractive index and larger range of transparency [13], metallic purities and high surface area for better sensitivity [14]. Evaporating conditions can slightly influence the MgF_2 because of their stability. In this connection, the silver and gold nanoparticles have satisfied responses in RI and higher sensitivities [15]. SPR signals are highly sensitive with different dielectric medium's refractive indices with closer metal surface and optical thickness varieties. The commonly used metal film in SPR is Au or silver because of their reliability and chemical stability [16]. Silver occupies obvious dip of response, higher resolution and scattering efficiency, narrower bandwidth with lower cost than gold [17]. Besides, silver generates stimulated SPR curve which provides stronger selectivity with higher sensitivity in SPR image detection [18]. In addition, silver is less costly than gold which reduces the fabrication budget. In spite of having advantages over gold, silver has some drawbacks like chemical instability and working limitations, because it can only work when it is covered with the thin film layer [19]. However, limitations of Ag and Au coating existed in sensitivity detection could be solved by involved in D-Shape [20] models. Metal layer of D-shaped LR-SPR can be grated to the adjacent core [21]. Besides the materials, dielectric also exploits LRSPR performance with its atomic consistency, exciting and thermal features [22].

In 2012, Chabot et al. reported a LRSPR sensor with 121 RIU^{-1} for the detection of living cells [23]. In 2013, Méjard et al. proposed a LRSPR sensor for biosensing application with high sensitivity response of 466 RIU^{-1} [24]. In 2017, Chaurasia et al. represented a LRSPR based sensor applying new theoretical approach for the enhancement of sensitivity [25]. In the same year, Hou et al. reported a multi layer based LRSPR sensor [26]. But, Jiang et al. proposed and fabricated hollow fiber based LRSPR sensor with sensitivity response of 2000 to 6600 nm/RIU [27]. In addition to biosensor, lots of refractive index based LRSPR sensors are proposed. In 2018, Pailwal et al. reported RI based MgF_2 and Au embedded LRSPR sensor for glucose monitoring [28]. Yearlier of 2020, Jain et al. reported LRSPR based sensor for gas sensing [29]. In very recent, D-shaped LRSPR based sensor is proposed and fabricated with sensitivity response of 947.31 nm/RIU [30]. Now, it can be concluded that there is still room to design new LRSPR based sensor for gaining high sensitivity response.

In this article, D-shaped MgF_2 and Ag materials embedded LRSPR based sensor is proposed and fabricated. The experimental outcome indicate the highest sensitivity of 1762.5 nm/RIU. This outcome undoubtedly says that this proposed sensor is a strong candidate in RI based sensing applications.

2. Theoretical and Numerical Simulation Analysis

The D-Shaped multilayer models based on LRSPR for single mode are simulated. For the completion of this work, theoretical and numerical explanation of the sensing analysis and calculation has been carried out. To point out the sensing performance in this work; some important parameters are required such as systematic method, simulated model design, optical properties with numerical expressions and sensitivity calculation. The analysis can be expanded by plotting the numerical expressions relevant to sensing based on LRSPR sensing mechanism.

2.1. Systematic Method for Simulation

The basic purpose of this D-Shaped LRSPR study is already discussed. To design and simulate the reported models, COMSOL Multiphysics 5.3a was used. COMSOL Multiphysics is contented cross-platform simulating software. The Multiphysics term states - it's a combination of various physical phenomena, Geomechanics module and user defined physics-based simulation. The 5.3 is an upgrade version of the COMSOL with some impressing applications. SPs (Surface Plasmons) can be inspected as an EMW (electromagnetic wave) which can propagate along with interface between the metal and buffer. Electromagnetic fields associated with surface plasmons at the resonance, reaches at its maximum interface. This electromagnetic field explicatively decays into metal and buffer. In this work, silver and gold has been used for better performance of the device. There is an analyte as substance helps to purify these metals because it is the purest substances. Figure 1 illustrates the experimental work based on deposition layer on side polished optical fiber. There are six models using two individual metals as Ag and Au are shows in Figure 1. In model-I there is a single metallic layer means the only layer is the metal layer. In model- II, a metallic layer over a dielectric (MgF_2) layer is deposited as (MgF_2/Ag) and (MgF_2/Au). In model-III, metallic layer of (Ag/Au) is covered by the dielectric layers. Therefore, two sandwich models such as ($MgF_2/Ag/MgF_2$) and ($MgF_2/Au/MgF_2$) are generated. As a dielectric, MgF_2 is thoroughly used for its stability and metallic purities. The use of this dielectric layer on the metal film purposely to prevent corrosion. MgF_2 as a dielectric function is helping to cut down the reflection. With a suitable reflective index, it can be optically applied as anti-reflective coating.

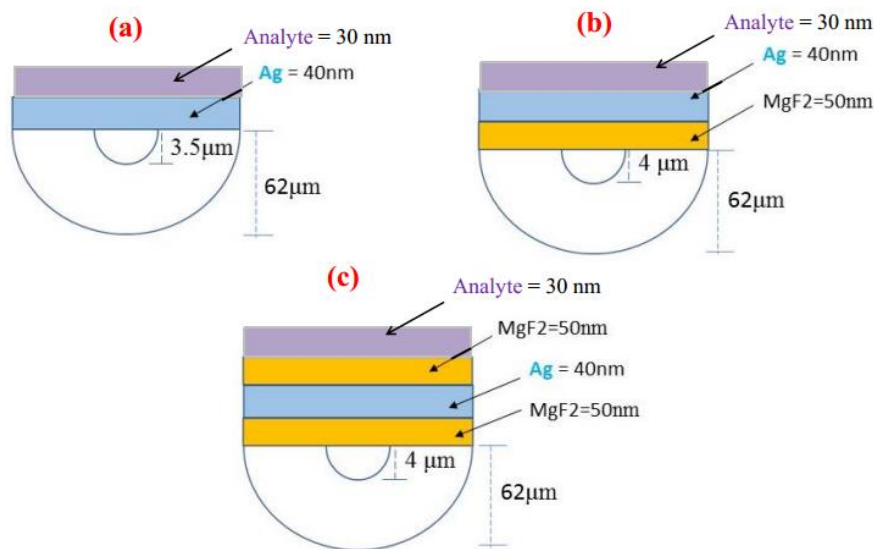


Fig 1. Proposed Simulation Models for experimental work using metallic Ag and Au. (a) model-I with single metallic layer of Au or Ag and analyte layer (b) model-II with dielectric $MgF_2/Ag/Analyte$ layers (c) model-III with $MgF_2/Ag/MgF_2/Analyte$ layers. Same types of models are also designed by replacing Au in the place of Ag.

Depending on the light, hits the core there are three categorized modes. When the light just passes through the core without hitting the cladding or layers it's called the core mode. Similarly, when the light passes through the layer it indicates as SPP mode. Unlike these, if light hit both the core and layer, the arisen mode is called as coupling mode. Coupling mode is nothing but the combination of both the core and SPP mode.

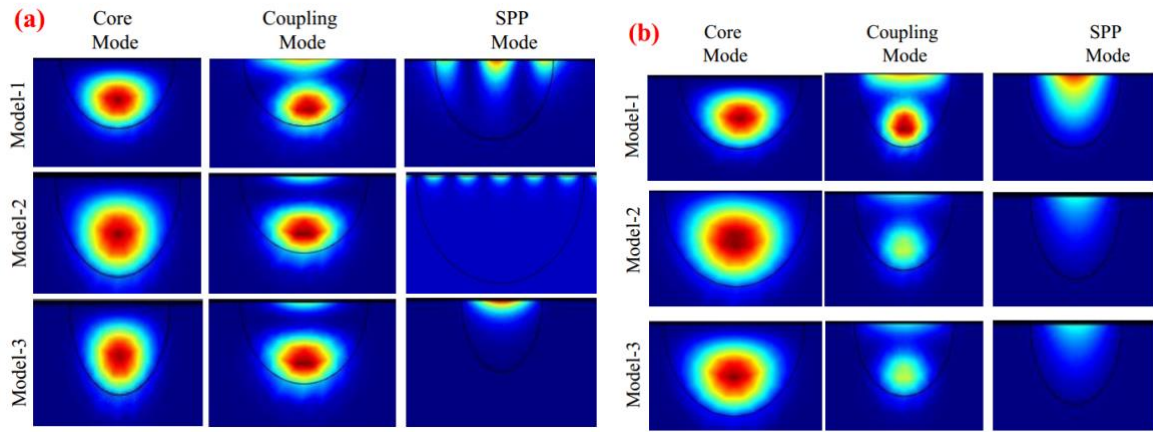


Fig 2. Mode fields distributions (Core mode, coupling mode and SPP mode) of the proposed simulation models based on metal (a) Ag and (b) Au.

Three of these modes from the proposed models are given in Fig 2. The figure shows for all three modes which is model -I for both metals are quite differentiative from the other two models. In fact, in model II and III, core and coupling mode for both the gold and silver metal is similar. In case of silver metal model II and III have almost the same coupling and SPP mode.

2.2 Optical properties and Empirical Exploration

LRSPR is generated when the light has interactions with thin metal films or any kind of nano featured strips such as nanoholes, nanoparticles, or nano shells. The wavelength range stands for this proposal augmented between 450 nm-850 nm which is considered to be an efficient range for LRSPR. At every succession for this range 20 nm has been increased. The diameters for core (8 μ m) and cladding (125 μ m) are cordially experienced. The metal films of Ag and Au with a thickness of 40 nm have also been applied. On the other hand, the thickness of analyte and MgF₂ layers are 30 nm and 50 nm respectively.

The design and fabrication of wavelength modulated LRSPR sensor with metal and buffer layer are reported. Now, the equations related to the approach are considered. The analyte is added to support the thin metal film in every structure. The surrounding refractive indexes of analyte are 1.33, 1.34, 1.35, 1.36, 1.37, and 1.38 and for dielectric layer MgF₂ is 1.38 as these are precise refractive index for evanescent property. MgF₂ is naturally birefringent, an ideal material that applied in the models as a buffer which work for the betterment of sensitivity. The foundation of LRSPR fabrication is the core therefore the material used there is called foundation material as because core is the base of simulation. The core material is the pure silica where the cladding material is doped silica. In accordance to the dispersion law of Sellmeier, refractive indices variance of silica can be expressed as

$$n(\lambda) = \sqrt{1 + \frac{B_1\lambda^2}{\lambda^2 - C_1} + \frac{B_2\lambda^2}{\lambda^2 - C_2} + \frac{B_3\lambda^2}{\lambda^2 - C_3}} \quad (1)$$

Here $n(\lambda)$ is the effective RI of silica for proposed wavelength. The Sellmeier coefficients follow: $B_1 = 0.696163$, $B_2 = 0.4079426$, $B_3 = 0.897479400$, $C_1 = 4.67914827 \times 10^{-3} \mu\text{m}^2$, $C_2 = 1.35120621 \times 10^{-2} \mu\text{m}^2$, $C_3 = 97.9240025 \mu\text{m}^2$ and $B_1, B_2, B_3, C_1, C_2, C_3$ are the coefficients of Sellmeier. After the silica, the next most important refractive indices are for the metal layer. Even if the silica is the foundation material for the structures, as for the layers, the metal is the base. The two effective metal Ag and Au have many refractive indices according to various equations. For this experiment, the Drude and Loentz both equations are conjointly used for the refractive indices.

The Drude (D) and Lorentz (L) combination are known for electronic transitions where former one depicts the intra-band and later inter-band respectively. The DL (Drude-Lorentz) conjunction overcomes the single D or L limitation. The DL model efficiently works between the wavelengths of

500 nm to 1000 nm [31]. The thin film metals (Au & Ag) material dispersion represented by DL equation which can be expressed as,

$$\varepsilon = \varepsilon\alpha - \frac{\omega^2 D}{\omega(\omega + j\gamma D)} - \frac{\Delta\varepsilon \cdot \Omega L^2}{\omega^2 - \Omega^2 L + i\Gamma L \omega} \quad (2)$$

These symbols have significance by their own meaning. ε is the metal permittivity where $\varepsilon\alpha$ is the permittivity for high frequency, $\omega = 2\pi c/\lambda$ which stands for angular frequency, ωD and γD indicate plasma frequency and damping frequency. $\Delta\varepsilon$ is for the weighting factor, ΓL is spectral width and ΩL is the oscillator strength respectively. Particular values for each and every symbolic parameter are given in Table 1.

Table 1: Parameter values used in Drude-Lorentz equation for both Ag and Au thin film:

Metal	ε	$\omega_D/2\pi$	$\gamma_D/2\pi$	$\Omega_L/2\pi$	$\Gamma_L/2\pi$	$\Delta\varepsilon$
Ag	2.4064	2214.6 THz	4.8 THz	1330.1 THz	620.7 THz	1.6604
Au	5.9673	2113.6 THz	15.92 THz	650.07 THz	104.86 THz	1.09

The main goal of this study is to achieve the better sensitivity of proposed D-Shaped LRSR. In this manner, the polarizations for the designed models were under consideration. Two major directions are the x-polarization and y-polarization. The differences between two modes are visible. Once the two modes of values (real and imaginary) are evaluated, the refractive indices difference between these two polarizing modes or Birefringence can be derived from

$$B = \Delta n = |n_x^i - n_y^i| \quad (3)$$

Here, B stands for birefringence and Δn is the RI difference between two modes with wavelength variation. n_x and n_y indicate the real refractive index values in x and y polarization modes. For any kind of plasmonic structures, a problem called confinement loss arises which cannot be expelled from the structures. Basically, a confinement-loss depicts the sensitivity of a structure. The calculation of this confinement-loss of a proposed model can be expressed as the equation (4) [32].

$$\alpha c(\text{dB/cm}) = 8.686 \times \frac{2\pi}{\lambda} \times 10^4 \quad (4)$$

Where, λ denotes operating wavelength of the reported structures and $\pi=3.1416$ is considerably standard. Coupling length states the minimal length to which maximal light amount passes through the silica core. The coupling length can be calculated by the equation (5) [32].

$$L_c(\mu\text{m}) = \frac{\lambda}{2|n_x^i - n_y^i|} \quad (5)$$

Herein, L_c indicates the proposed coupling length and λ is the wavelength where two of these are inversely proportional to each other. An optical strip passes the mono core enabled by the reported structure. It supports better Long-Range Surface Plasmon Resonance sensing. The output power can be derived from equation (6) [32].

$$P_{out}(\lambda) = \sin^2 \left(\frac{|n_x^i - n_y^i| \pi L}{\lambda} \right) = \sin^2 \left(\frac{\Delta n_{xy} \pi L}{\lambda} \right) \quad (6)$$

Whither, L represents the entire length of designed fiber. Another term which depends upon the output power is called transmittance spectrum. When the light exceeds by the supposed fiber, it can be calculated by equation (7) [32].

$$T_r = 10 \log_{10} \left(\frac{P_{out}}{P_{in}} \right) \quad (7)$$

Here, both P_{in} and P_{out} are indicating the power at their maximum for input and output respectively. Where, the visual power transmittance or optical power of a specific structure is defined by T_r . However, wavelength sensitivity of a proposed sensor evaluation through the switch of the sharpness at its maximum transmittance curve at a specified wavelength because of the absolute variation of refractive indices. The wavelength sensitivity can be calculated by the equation (8) [32].

$$S_w \left[\frac{nm}{RIU} \right] = \frac{\Delta \lambda_p}{\Delta n} \quad (8)$$

Here, S_w defines the sensitivity wavelength measured in nm/RIU and λ_p defines the peak wavelength with variance in other words, resonance wavelength. Δn denotes the refractive indices variance. The sensitivity measured with various transmittance curve or Tr by the equation (9) [32].

$$S_v \left[\frac{dB}{RIU} \right] = \frac{\max(tx_{b_1} - tx_{b_2})}{\max(n_{b_1} - n_{b_2})} \quad (9)$$

In order that, Δn_{b_1} is the difference between refractive indices and tx_{b_1} & tx_{b_2} are the transmittance curve of maximal amplitude of b_1 , b_2 respectively. Any changes in the RI can be detected by the resolution variance of the reported structures. For this proposed model the resolution can be easily calculated by equation (10) [33].

$$RI[RIU] = \frac{\Delta n \times \Delta \lambda_{min}}{\Delta \lambda_{peak}} \quad (10)$$

Here, Δn indicates the refractive indices difference, $\Delta \lambda_{min}$ and $\Delta \lambda_{peak}$ are the differences between minimum wavelength and peak wavelength respectively. The phase detecting method is directly affected by the sensor resolution to oppose the amplitude interrogating method. The complications of this method can be extracted by applying the sensitivity equation of amplitude. This sensitivity can be spontaneously evaluated by the equation (11) [34].

$$S_a[RIU^{-1}] = - \frac{1}{\alpha_c} \times \frac{\Delta \alpha_c}{\Delta n} \quad (11)$$

Where, α_c is the confinement loss. $\Delta \alpha_c$ and Δn represent the difference between confinement-loss and refractive indices respectively. Equations from 6 to 11 play a vital rule for measuring the sensitivity in LRSPR sensor. Both confinement loss and transmittance have great impacts on sensing analysis, these two are the key point for sensitivity. Sensitivity based on LRSPR sensor can be calculated with any of this two, as long as none of these are calculated, sensitivity is impossible.

2.3 Simulated Sensitivity Measurement

The experimental measurement of sensitivity is the main approach for this simulation. The target simulation attempt is the sensitivity performance which relies on several terms and conditions. The buffer layer and the thin metal type is also vulnerable. Another inspection is the effect of metal-film thickness and material properties on the spectral-phase performance. Here, the simulated sensing analysis is carried out for three different models. In this work, transmittance is used to evaluate the ultimate sensitivity, which can be calculated by applying Equation (7) which also plotted in Fig 3. The transmittance is one of the operations obtain, while the light wave hits the core or pass through the surface. The transmitted light is polarized along with the axis of the polarizer. The two main cases of axis are X and Y. These are also called as X and Y polarizations. According to the structures there are different layers in different models. So, the more the layers in a model, the more assistance the polarization gives to distinguish the sensitivity performance as in the model. As illustrated in Figure 3, both silver and gold exhibit transmittance with wavelength variance. For each models the silver-based graphs are sharper and more promising than the gold-based models. The transmittance has been increased with the wavelengths until reaching the proposed limit. From Figure 3, it is also viewed that both model-1 and model-2 for two defined metals have same transmittance range but for the sandwich model or model-3 transmittance are different from each other. The transmittance for silver-based sandwich structure has shorter range than the gold based one.

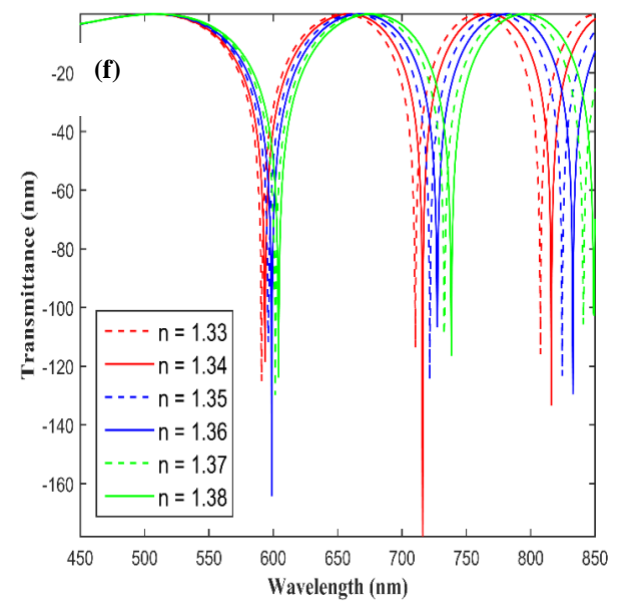
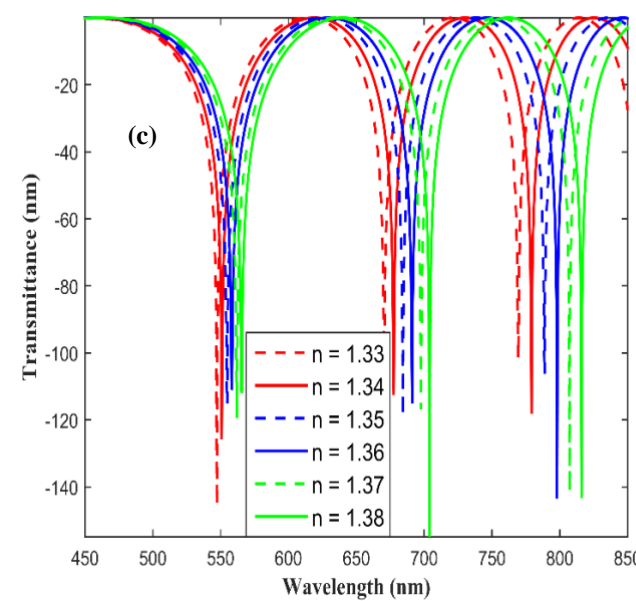
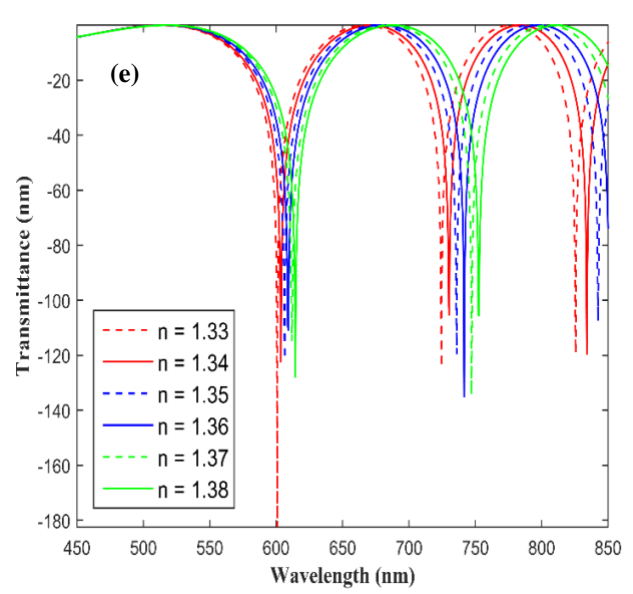
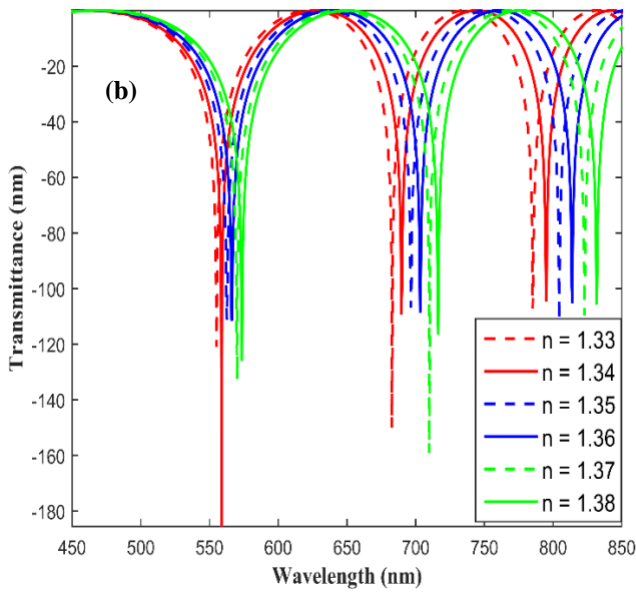
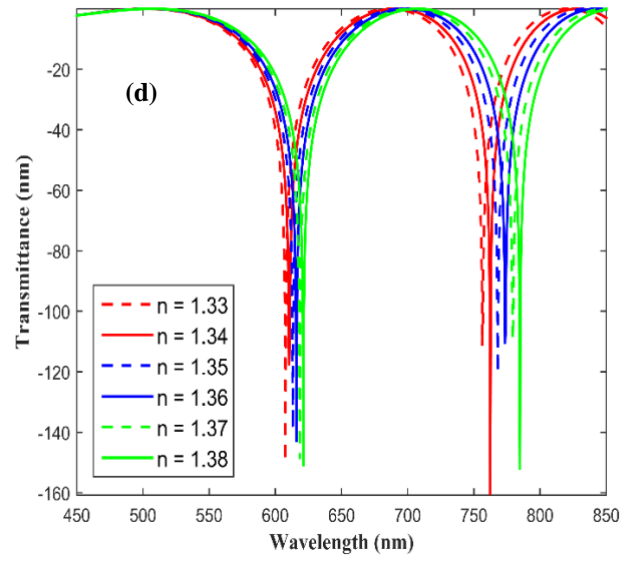
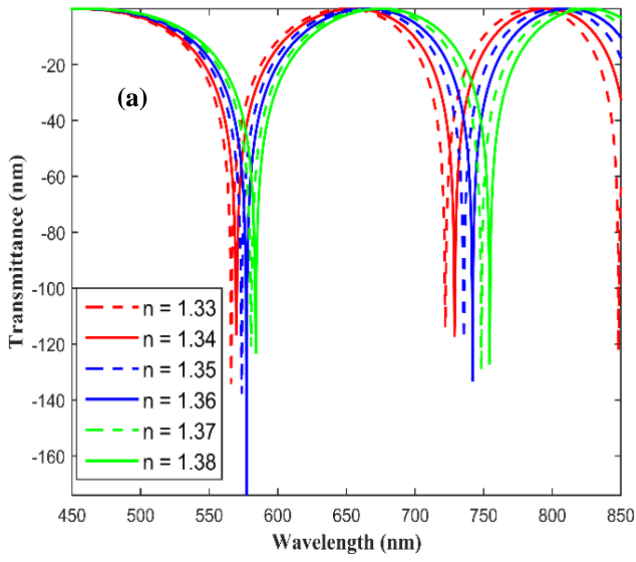
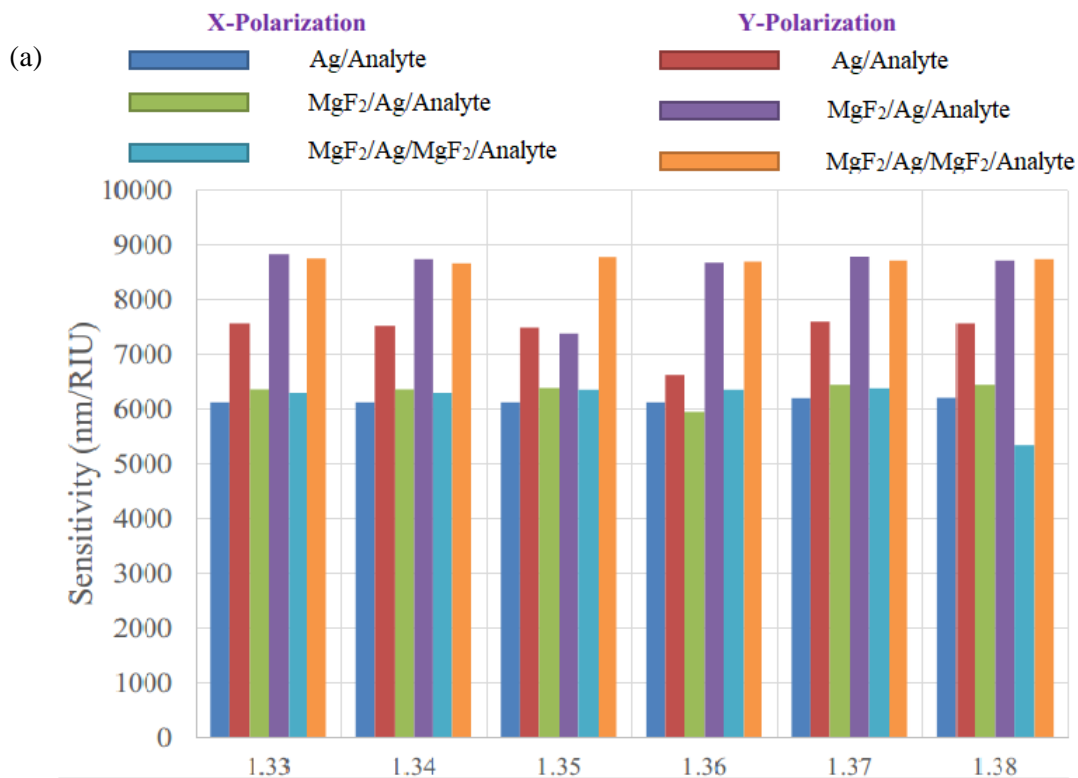


Fig 3: Transmittance vs wavelength performances. Based on Ag (a) model 1 (b) mode 2 (c) model 3 or sandwich model and based on Au (d) model 1 (e) model 2 (f) model 3 for sandwich structure

The resonant wavelength shifts to longer wavelength when the refractive indices of analyte increase. The spectral-phase sensing performance in a sample shows refractive index with dynamic range of 1.33-1.38 using both metals of Ag and Au for long-range SPR configurations. Sensitivities between the transition regimes, are very low. Specific combinations of Ag and Au with buffer layer, the sensitivity magnitude can extremely be high. The sensitivities plotted in Figure 4. Best x and y polarizing sensitivity limit the detection on changes analyte refractive indices 1.33 to 1.38. For silver, the sensitivity varies from 5.34×10^3 nm/RIU to 8.34×10^3 nm/RIU for x and y polarization and for gold 6.03×10^3 nm/RIU to 7.89×10^3 nm/RIU for those polarizations. Simulation results indicate that spectral-phase Long range SPR sensing performance is not equally sensitive to the different models using the same metal. From Figure 4, it can be seen that silver based simulated sensitivities for both x and y polarization are more vacillating than the gold-based simulation. In silver-based sensitivities, this fluctuation is more at 1.38 of RI than the remaining RI's. Also, as previously mentioned silver gives higher and sharper sensitivities than gold. From Figure 4, it is an evidence to this argument that silver metal is conciliating enough to be compared with gold. Even with silver, model-2 and model-3 are work much better than the model-1.

Well, from here, the polarized lights are to be measured from the physical processes of deviated light beams, which also known as birefringence (the property of double refraction). When the polarized light waves hit the surface, it will be transmitted and reflected. As per the sensitivity of this work measured from transmittance, this term should be dealt with. The more the layers assist the light to transmit in the cases (both x and y polarization) for linear polarization, the more it helps to distinguish the sensitivity performance according to the layers.



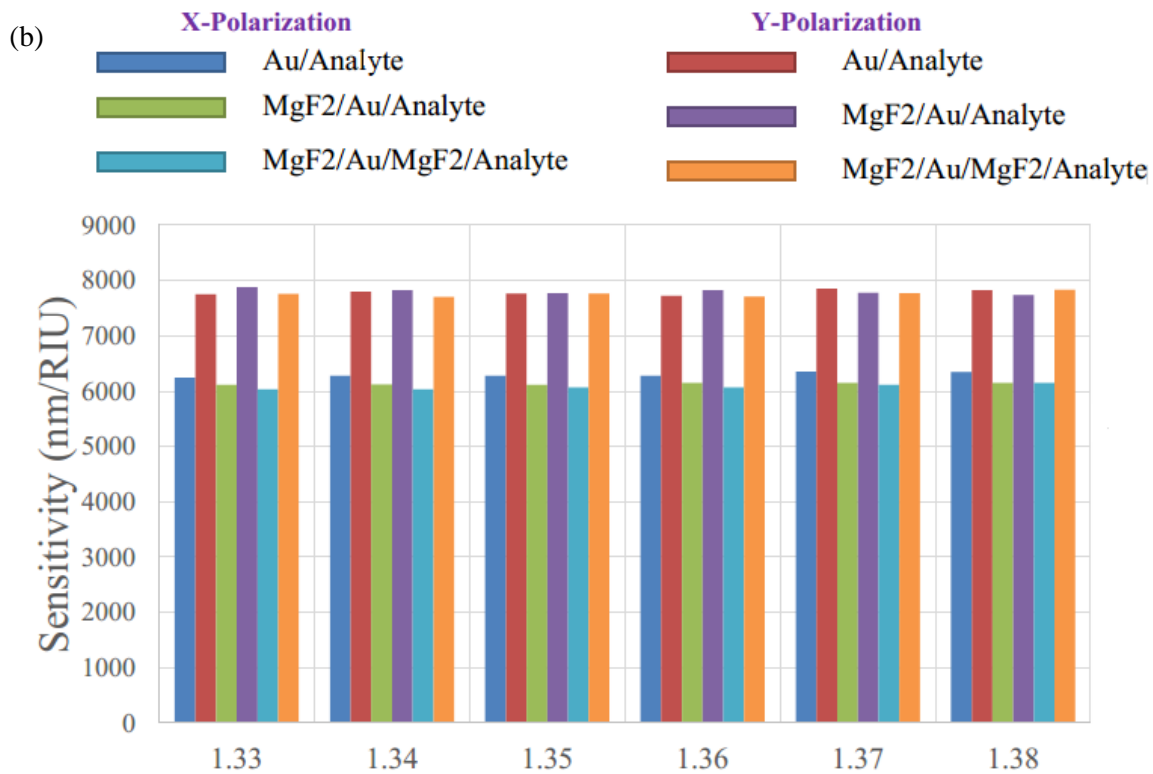


Fig 4: Sensitivities vs. analyte performances. Based on Ag (a) sensitivities for combined models I, II and III. Based on Au (b) sensitivities for combined models I, II and III.

3. Experimental Sensitivity Measurement

For this part, there are processes to strengthen the LRSR phenomena before getting into the sensing method. Basically, there are three main processes in this experiment. Firstly, optical fiber will undergo wheel polishing method to establish a D-shape fiber. Secondly, the D-shape region is deposited with layers of metal and DBL to establish a sensing surface. Lastly is the sensing method and collection of experimental data.

Firstly, a single-mode optical fiber (SMF) is used while processing. The SMF was stripped at the middle exposing cladding/core region and was put at a wheel polishing setup consist of clipper for holding both end of the fiber. Blank driller attached with fine and coarse sandpaper for grinding the SMF. At one end of the fiber, a light source is connected to allow light flowing so that at another end of the fiber, a power meter connected will measure the amount of power loss while grinding the fiber. The amount of power loss was set to ~6 dB loss. Thus, it can be predicted that a large amount of light was leaked at the sensing region, which in turn will enhance light interaction thus increasing its sensitivity. The resulting of the polishing is schematically drawn in Fig. 5. The diameter of cladding/core of the fiber will be changed from the original of 125 μm , and it is measured with an optical microscope.

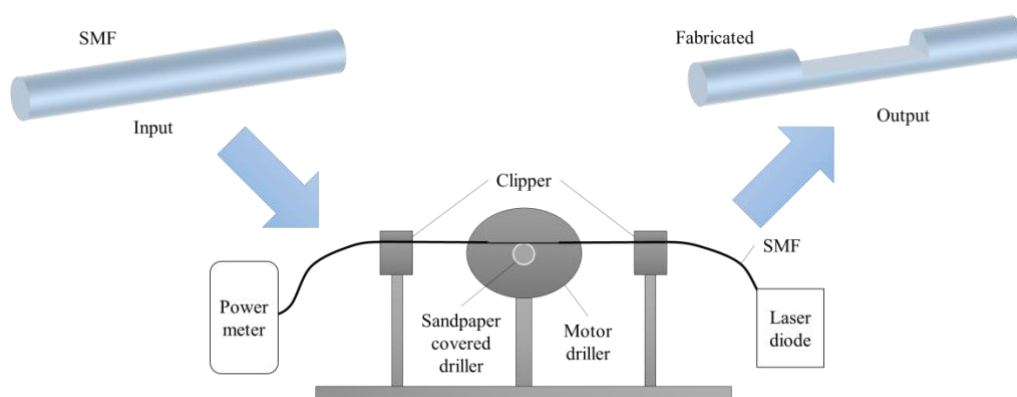


Fig 5: Schematic diagram of resulted Wheel Polishing Method

After the D-shape fiber is finished, it will undergo deposition of thin metal and DBL. the deposition process was done using an electron beam evaporation machine (e-beam). The deposition was done in two sets; DBL/metal layer, and DBL/metal/DBL layer, for which conventional LRSPR (cLRSPR) and symmetric LRSPR (sLRSPR) represented gradually. For this experiment, MgF₂ was used as DBL and the thin metal film was silver (Ag). Since Ag is a noble metal, it possesses a strong absorption in ultraviolet region thus suitable for plasmonic study. The thickness for MgF₂ and Ag were constantly set to 50 nm and 40 nm for all DBL and thin metal deposition. Thus, the configuration of cLRSPR and sLRSPR would be [50 nm- MgF₂/40 nm-Ag] and [50 nm- MgF₂/40 nm-Ag/50 nm-MgF₂] respectively.

When all the fabrication processes are done, then it is moved to the sensing process (details in Fig. 6). For this process, sensitivities towards the change of refractive index (RI) are investigated. Thus, solution of different RI is prepared, specifically using glucose solution, since it is easiest to prepare. The glucose powder is mixed with DI water using mass-to-volume ratio. The RI of the solution is verified using a lab standard refractometer. Next, fabricated fiber was connected to a white light source and a spectrometer (HR4000 Ocean Optics) at both end and the setup was in a stable position. The spectrometer is connected to a computer and the light transmittances were recorded and analyzed using Spectra Suit software.

Whenever a metal layer is sandwiched in between two distinguishable dielectric buffer layers (DBL) with similar refractive index (RI), two types of propagating modes will be generated due to the overlapping of surface plasmon polaritons (SPPs) within a metal layer interface. These modes are known as long-range SPPs (LRSPPs) and short-range SPPs (SRSPPs) [5, 10] and it is called LRSPR and SRSPR respectively. As soon as they triggered the resonance phenomenon which occur with the presence of the evanescent wave. As a result, there will be two dips rise out from the resonance spectra of LRSPR sensor which are long-range and short-range resonance dip as shown in Fig.7.

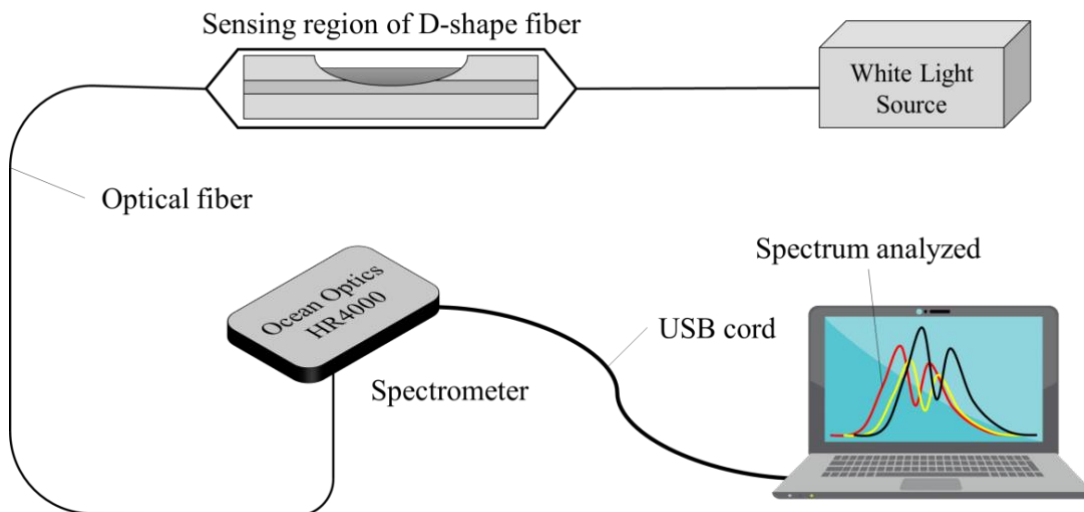


Fig 6: Sensing process for D-shape fiber

They could be differentiated by the loss, as SRSPPs suffer bigger loss which can make the LRSPPs secure with some advantages on preserving the loss. Thus, the LRSPPs possess narrower and deeper dip which directly improve the sensor parameters such as detection accuracy (DA) and high sensitivity when external environment face changes in RI [11].

Hence, only long-range dip is chosen to characterize for sensor purpose. The RI of DBL will determine the behavior of LRSPR sensor as the closer the external environment RI to the RI of DBL, the more significant it affects the long-range. Therefore, it is proven that the sensitivity of the sLRSPR sensor improve at value around 1762.5 nm/RIU when the external environment RI at range 1.37-1.38 comparing to its sensitivity of resonance sensor at RI range 1.33-1.34 which is 1250 nm/RIU. In addition, the penetration depth of the dip at this RI range (1.37-1.38) is deeper comparing to the dip at RI range (1.33-1.34). The occurrence is due to the material of DBL (MgF₂) in which the

RI range is about 1.374-1.384 corresponding to the wavelength range between 400 nm-1000 nm [9].

Table 2. Comparison of performance parameters among different sensors between two different RI (1.33-1.34).

Type of Sensor	cLRSPR	sLRSPR
Sensitivity (nm/RIU)	2812.5	1250
FOM (RIU ⁻¹)	78.23	69.44
FWHM _{avg} (nm)	35.95	18

Table 3. Comparison of performance parameters among different sensors between two different RI (1.37-1.38)

Type of Sensor	sLRSPR
Sensitivity (nm/RIU)	1762.5
FOM (RIU ⁻¹)	41.59
FWHM _{avg} (nm)	42.375

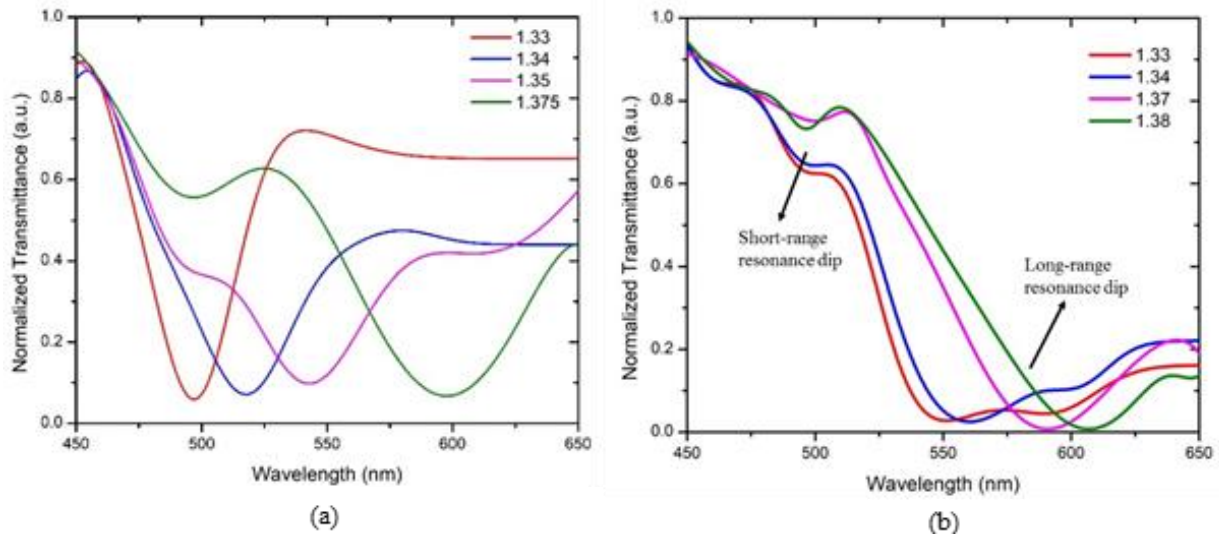


Fig 7: Graph of transmittance spectra of the sensor as a function of wavelength (a) resonance wavelength of cLRSPR range from 450-650 nm at RI range 1.33-1.35 and 1.375 and (b) resonance wavelength of sLRSPR at refractive index range from 450-650 nm at RI range 1.33-1.34 and 1.37-1.38

Apart from that, cLRSPR sensor also has been studied where the configuration is formed of two layers, MgF₂/Ag which refer to Model II in Figure I. The series of RI range starting from 1.33, 1.34, 1.35 and 1.375 have conducted in the experiment where the first two RI (1.33 and 1.34) are maintained along the study and the last two RI (1.35 and 1.375) are an addition of RI that able to capture to give the significant affect towards the LRSPR dip. It can be observed that the penetration depth and sensitivity of the cLRSPR sensor, 2812.5 nm/RIU is better at RI range, 1.33-1.34 compared to sLRSPR sensor. Literatures reported that the thicknesses of DBL which usually used are around 200-600 nm using MgF₂ [4] and 300-500 nm for using Teflon [25] This might be the reason on the results that cLRSPR is better here since the thickness of DBL is 50 nm. By introducing the MgF₂ in the system, it is proven that the generated long-range (cLRSPR) is capable to enhance the sensitivity of cSPR sensor, 2166.67 nm/RIU at RI range 1.33-1.34 by $\Delta 645.833$ nm/RIU and within the sLRSPR sensor itself, the sensitivity at RI range 1.37-1.38, 1762.5 nm/RIU surpass the sensitivity at RI range 1.33-1.34, 1250 nm/RIU by $\Delta 512.5$ nm/RIU which indicate that the RI of DBL play an important role for sensitivity performance. Tables 2 and 3 represent the experimental outcomes summary of the proposed LRSPR sensor.

4. Conclusion

Extensive experimental analysis for various D-shaped models based on LRSPR sensors are expounded with this report. Models presented in this article are the inception of LRSPR sensor simulation. The entire study is based on the fabrication of those following proposed models consisting Ag. Through the theoretical and numerical analysis, the simulated sensitivities using Ag and Au materials are measured. The sensitivities have also been evaluated experimentally using silver material for its standardized performance than gold. The RI ranges of 1.33, 1.34, 1.35 and 1.375 have conducted in the experiment which the first two RI (1.33 and 1.34) are maintained along the study and the last two RI (1.35 and 1.375). The experimental measurements are balanced with the simulated result analysis. Characteristics of DBL exploited for the refractive index measurement. The penetration depth and sensitivity of cLRSPR sensor is 2812.5 nm/RIU at RI range of 1.33-1.34, compared to sLRSPR sensor. The generated cLRSPR enhanced the sensitivity of cSPR sensor by 2166.67 nm/RIU at 1.33-1.34, 1762.5 nm/RIU exceeded the sensitivity at 1.33-1.34, 1250 nm/RIU by Δ 512.5 nm/RIU. Here, LRSPR offers better sensitivity for the metal silver. In LRSPR, cLRSPR is more tolerant than sLRSPR.

Acknowledgement:

The work is funded by IIRG grant from University Malaya (IIRG005B-19IIS).

Conflicts of interest/Competing interests

Authors claim no conflict of interests

References:

- [1] Vincent Chabot, Yannick Miron, Michel Grandbois, Paul G. Charette, "Long range surface plasmon resonance for increased sensitivity in living cell," *Sensors and Actuators B: Chemical*, vol. 174, pp. 94-101, 2012.
- [2] N.A.M. Zainuddin, M.M. Ariannejad, P.T. Arasu, S.W. Harun, R. Zakaria, "Investigation of cladding thicknesses on silver SPR based side-polished optical fiber refractive-index sensor," *Results in Physics*, vol. 13, p. 102255, 2019.
- [3] Li-Ye Niu, Qi Wang, Wan-Ming Zhao, Jian-Ying Jing, "High quality factor D-type fiber surface plasmon resonance (SPR) sensor based on the modification of gold nanoshells," *Instrumentation Science & Technology*, vol. 48, no. 1, pp. 63-74, 2020.
- [4] Banxian Ruan, Qi You, Jiaqi Zhu, Leiming Wu, Jun Guo, Xiaoyu Dai and Yuanjiang Xiang, "Improving the Performance of an SPR Biosensor Using Long-Range Surface Plasmon of Ga-Doped Zinc Oxide," *Sensors (Basel)*, vol. 18, no. 7, pp. 1-8, 2018.
- [5] P. Berini, "Long-range surface plasmon polaritons," *Advances in Optics and Photonics*, vol. 1, p. 484–588, 2009.
- [6] Hui Zhang, Yaofei Chen, Xinjie Feng, Xin Xiong, Shiqi Hu, Zhupeng Jiang, Jiangli Dong, Wenguo Zhu, Wentao Qiu, Heyuan Guan, Huihui Lu, Jianhui Yu, Yongchun Zhong, Jun Zhang, Miao He, Yunhan Luo, and Zhe Chen, "Long-Range Surface Plasmon Resonance Sensor Based on Side-Polished Fiber for Biosensing Applications," *IEEE JOURNAL OF SELECTED TOPICS IN QUANTUM ELECTRONICS*, vol. 25, no. 2, pp. 1-9, 2019.
- [7] Fuzi Yang, J. R. Sambles, and G. W. Bradberry, "Long-range surface modes supported by thin films," *The American Physical Society*, vol. 4, no. 11, pp. 5855-5872, 1991.
- [8] Chenyuan Li, Binbin Song, Yu Guo, Jixuan Wu, Wei Huang, Xujie Wu, Chang Jin, Shengyong Chen, "Two Modes Excited SPR Sensor Employing Gold-Coated Photonic Crystal Fiber Based on Three-Layers Air-Holes," *IEEE Sensors Journal*, vol. 20, no. 11, pp. 5893 - 5899, 2020.
- [9] Jian-Ying Jing, Si-Yuan Li, Xue-Zhou Wang, Qi Zhu, Fan-Li Meng, Qi Wang, "A D-type fiber based symmetrical long-range surface plasmon resonance sensor with high quality factor," *Measurement*, vol. 140, pp. 395-406, 2019.
- [10] D. Sarid, "Long-Range Surface-Plasma Waves on Very Thin Metal Films," *Physical Review LETTERS*, vol. 47, no. 26, pp. 1927-1930, 1981.
- [11] J. Homola, "Surface Plasmon Resonance Sensors for Detection of Chemical and Biological Species," *Chemical Reviews*, vol. 108, no. 2, pp. 462-493, 2008.

- [12] Damra E. Mustafa & Tianming Yang & Zhou Xuan & Shizhen Chen & Haiyang Tu & Aidong Zhang, "Surface Plasmon Coupling Effect of Gold Nanoparticles with Different Shape and Size on Conventional Surface Plasmon Resonance Signal," *Plasmonics*, vol. 5, no. 3, pp. 221-231, 2010.
- [13] Gong Zhang, Xiuhua Fu, Shigeng Song, Kai Guo and Jing Zhang, "Influences of Oxygen Ion Beam on the Properties of Magnesium Fluoride Thin Film Deposited Using Electron Beam Evaporation Deposition," *Coatings*, vol. 9, pp. 834-845, 2019.
- [14] Prattay D. Kairi, Mustafizur Rahman, Emran Khan Ashik, Quazi D.M. Khosru, "A novel technique for detection of biomolecules and its aqueous concentration using a double gate graphene field effect transistor," *Sensing and Bio-Sensing Research*, vol. 19, p. 7–13, 2018.
- [15] Jinying Ma, Kun Liu, Junfeng Jiang, Tianhua Xu, Shuang Wang, Pengxiang Chang, "All optic-fiber coupled plasmon waveguide resonance sensor using ZrS₂ based dielectric layer," *Optics Express*, vol. 28, no. 8, pp. 11280-11289, 2020.
- [16] Jilí Homola, Hana Vaisocherová, Jakub Dostálek, Marek Piliarik, "Multi-analyte surface plasmon resonance biosensing," *Anal Bioanal Chem*, vol. 387, pp. 1449-1458, 2007.
- [17] Saeid Nazem, Mohammad Malekmohammad, Mahmood Soltanolkotabi, "Theoretical and experimental study of a surface plasmon sensor based on Ag MgF₂ grating coupler," *Applied Physics B*, vol. 126, no. 5, pp. 1-11, 2020.
- [18] Nak-Hyeon Kim, Munsik Choi, Tae Woo Kim, Woong Choi, Sang Yoon Park, "Sensitivity and Stability Enhancement of Surface Plasmon Resonance Biosensors Based on a Large-Area," *Sensors (Basel)*, vol. 19, no. 8, pp. 1894-1902, 2019.
- [19] Sabine Szunerits, Xavier Castel and Rabah Boukherroub, "Surface Plasmon Resonance Investigation of Silver and Gold Films Coated with Thin Indium Tin Oxide Layers: Influence on Stability and Sensitivity," *Physical chemistry*, vol. 112, no. 40, p. 15813–15817, 2008.
- [20] M. Mitsushio, K. Miyashita, M. Higo, "Sensor properties and surface characterization of the metal-deposited SPR optical fiber sensors with Au, Ag, Cu, and Al," *Sensors and Actuators a-Physical*, vol. 125, pp. 296-303, 2006.
- [21] Famei Wang, Chao Liu, Zhijie Sun, Tao Sun, Banghua Liu, Paul K. Chu, "A Highly Sensitive SPR Sensors Based on Two Parallel PCFs for Low Refractive Index Detection," *IEEE Photonics Journal*, vol. 10, no. 4, pp. 1-11, 2018.
- [22] Zhaoxian Su, Jianbo Yin and Xiaopeng Zhao, "Terahertz dual-band metamaterial absorber based on graphene/MgF₂ multilayer structures," *OPTICS EXPRESS*, vol. 23, no. 2, pp. 1679-1690, 2015.
- [23] Chabot V, Miron Y, Grandbois M, et al. Long-range surface plasmon resonance for increased sensitivity in living cell biosensing through greater probing depth. *Sens Actuators B Chem* 2012;174(11):94–101.
- [24] Méjard R, Dostálek J, Huang C J, et al. Tuneable and robust long-range surface plasmon resonance for biosensing applications. *Opt Mater* 2013;35(12):2507–13.
- [25] Chaurasia D, Goswami N, Saha A. Long range surface plasmon resonance based taper fiber optic sensor with enhanced sensitivity using Au nano-layer through radially polarized light. In: *Proceedings of the conference series: materials science and engineering*; 2017.
- [26] Hou C, Galvan DD, Meng G, et al. Long-range surface plasmon resonance and surface-enhanced Raman scattering on X-shaped gold plasmonic nanohole arrays. *Phys Chem Chem Phys* 2017;19(35):24126
- [27] Jiang Y X, Liu B H, Zhu X S, et al. Long-range surface plasmon resonance sensor based on dielectric/silver coated hollow fiber with enhanced figure of merit. *Opt Lett* 2015;40(5):744–7.
- [28] Paliwal, A., Tomar, M. and Gupta, V., 2019. Refractive index sensor using long-range surface plasmon resonance with prism coupler. *Plasmonics*, 14(2), pp.375-381.
- [29] Jain, S., Paliwal, A., Gupta, V. and Tomar, M., 2020. Long Range Surface Plasmons assisted highly sensitive and room temperature operated NO₂ gas sensor. *Sensors and Actuators B: Chemical*, 311, p.127897.
- [30] Wang Q et al. A D-Shaped Fiber Long-Range Surface Plasmon Resonance Sensor with High Q-Factor and Temperature Self-Compensation, *IEEE TRANSACTIONS ON INSTRUMENTATION AND MEASUREMENT*, 2020; 69 (5): 2218-2224.
- [31] Dominique Barchiesi and Thomas Grosge, "Fitting the optical constants of gold, silver, chromium, titanium, and aluminum in the visible bandwidth," *Journal of Nanophotonics*, vol. 8, pp. 083097-083114, 2014.

[32] Jabin, M.A., Luo, Y., Peng, G.D., Rana, M.J., Ahmed, K., Nguyen, T.K., Paul, B.K. and Dhasarathan, V., 2020. Design and fabrication of amoeba faced photonic crystal fiber for biosensing application. *Sensors and Actuators A: Physical*, 313, p.112204.

[33] Jabin, M.A., Ahmed, K., Rana, M.J., Paul, B.K., Islam, M., Vigneswaran, D. and Uddin, M.S., 2019. Surface plasmon resonance-based titanium coated biosensor for cancer cell detection. *IEEE Photonics Journal*, 11(4), pp.1-10.

[34] Sharma, A.K. and B.D. Gupta, "Fibre optic sensor based on long-range surface plasmon resonance: a theoretical analysis.," *Journal of Optics A: Pure and Applied Optics*, vol. 9, no. 7, p. 682, 2007.